Int. J. Electrochem. Sci., 17 **(2022)** Article Number: 220671, doi: 10.20964/2022.06.56

International Journal of
ELECTROCHEMICAL
SCIENCE
www.electrochemsci.org

Preparation of high porous carbon using Al-based MOFs and influence of dimethylformamide on morphological and electrochemical supercapacitor performances

Qiuchen Wang, Bo Xiong, Junqing Pan[*]

State Key Laboratory of Chemical Resource Engineering, Beijing Advanced Innovation Center for Soft Matter Science and Engineering, College of Chemistry, Beijing University of Chemical Technology, Beijing 100029.
[*]E-mail: jqpan@buct.edu.cn

Received: 2 March 2022 / *Accepted:* 14 April 2022 / *Published:* 7 May 2022

Presently, a porous carbons (PC) derived from Metal-organic framework (MOF) has shown ewith excellent electrochemical performance for supercapacitor due to their special morphology and richly micro/mesoporous structure. Here a new activated PC (APC) derived from Al-MOF is reported via facile combined carbonization and KOH treatment. It is found that the morphology of Al-MOF is influenced by the different compositions of solutions. The shape of Al-MOF was gradually transformed from spherical to hexagonal by the addition of DMF content. The carbon electrode provides an advantageous specific capacitance (SC) of 342 F g^{-1} at 1 A g^{-1} in the 3 electrode system. Correspondingly, it also exhibits excellent durability with superior capacitance retention of 96% after 150,000 cycles at 50 A g^{-1}. This work suggests a new strategy to prepare electrode material with extreme performance for energy storage.

Keywords: Porous carbon, Metal-organic framework, Al-MOF, supercapacitor

1. INTRODUCTION

In recent years, many researchers have focused on developing new energy storage materials with renewable features and excellent properties due to the severe problems of environmental pollution by the massive consumption of fossil energy [1-4]. Supercapacitors have attracted wide attention due to their high power density, excellent durability, and low maintenance costs[5-7]. Supercapacitors are generally divided into electric double-layer capacitors (EDLC) and pseudocapacitors based on the charge and discharge mechanism. The former stores the charges on the interface of electrolyte and active material and oxidation-reduction reactions of the latter[8-10]. However, supercapacitors have certain practical limitations, such as safety being more challenging to control due to too fast charging speed and high discharge efficiency, which ultimately affects their practical application[11]. Recently,

porous carbons are high-quality electrode materials widely used in supercapacitors due to their excellent properties, such as tunable porous frameworks, high electrical conductivity, and excellent chemical stability. In previous research work, researchers used carbon nanotubes, carbon fibers, and carbon nanospheres as materials for supercapacitors[12-16].

MOFs are mainly constructed by coordinate bonds between metal ions and organic ligands, which serve as connection points and supporting frameworks, respectively[17-21]. Generally, MOFs have excellent thermal and chemical stability due to their strong carbon-carbon and metal-carbon bonding. Based on these excellent properties, MOFs and their derivatives have shown unique application prospects in many fields, such as energy storage and gas separation. [22-26]. Among these applications, MOF-derived APC has been employed as electrode materials for supercapacitors due to its advantages of higher specific surface area and rich porous structure, increased adsorption capacity and environmental protection. These beauties are very suitable for the penetration of electrolyte and electrolyte ions, leading to the enhanced performance of supercapacitors[27-30]. Aluminum (Al) is the most abundant metal element in the earth's crust. The research on new Al-MOF and the relevant APC is expected to reduce the cost of APC and increase the high-performance of supercapacitors [31].

In the present study, we proposed a new synthetic method of MOFs with different shapes using $Al(NO_3)_3 \bullet 9H_2O$ and Trimesic acid (BTC) as the starting materials under the adjustion of reaction times, temperatures, and solvents composition of the water, ethanol, and DMF. It is found that the shape of the Al-MOF was gradually transformed from spherical to hexagonal after adding the different dosages of DMF in the solvent. Subsequently, APC with a high specific surface area (SSA) was synthesized via the carbonization and activation of optimal Al-BTC. Furthermore, the APC supplied superior specific capacitances (SCs) of 324 and 252 F g^{-1} at current densities of 1 and 50 A g^{-1}, showing excellent rate performance. Additionally, it has superb cycling stability with satisfactory capacitance retention of 96% after 150,000 cycles at 50 A g^{-1}. This study shows that APC is a high-quality electrode material for supercapacitors with enhanced electrochemical properties.

2. EXPERIMENTAL SECTION

2.1. Preparation of porous carbon from Al-BTC

All chemicals were analytical reagent grade in the experiment. Firstly, 1.397 g of $Al(NO_3)_3 \bullet 9H_2O$ and 0.525 g of BTC were put into a 100 mL reaction vessel liner, 1:1:1 ethanol, deionized water, and DMF were added and kept stirring for 30 min. Subsequently, the solution was placed into an oven and heated at 130°C for 12 h. After that, The resultant product (marked as Al-BTC) was centrifuged 3-4 times with deionized water and ethanol to remove impurities and dried in the oven at 60℃ overnight. Afterward, the dried Al-BTC was set out in a nickel boat. It was heated at 800°Cin a nitrogen protected tube furnace for 2 h. Then, the resultant was micro-boiled with a 6 mol L^{-1} KOH solution for 1 h to remove metal ions, marked as Al-BTC-C. Finally, it was filtered and dried after it was cooled to obtain PC.

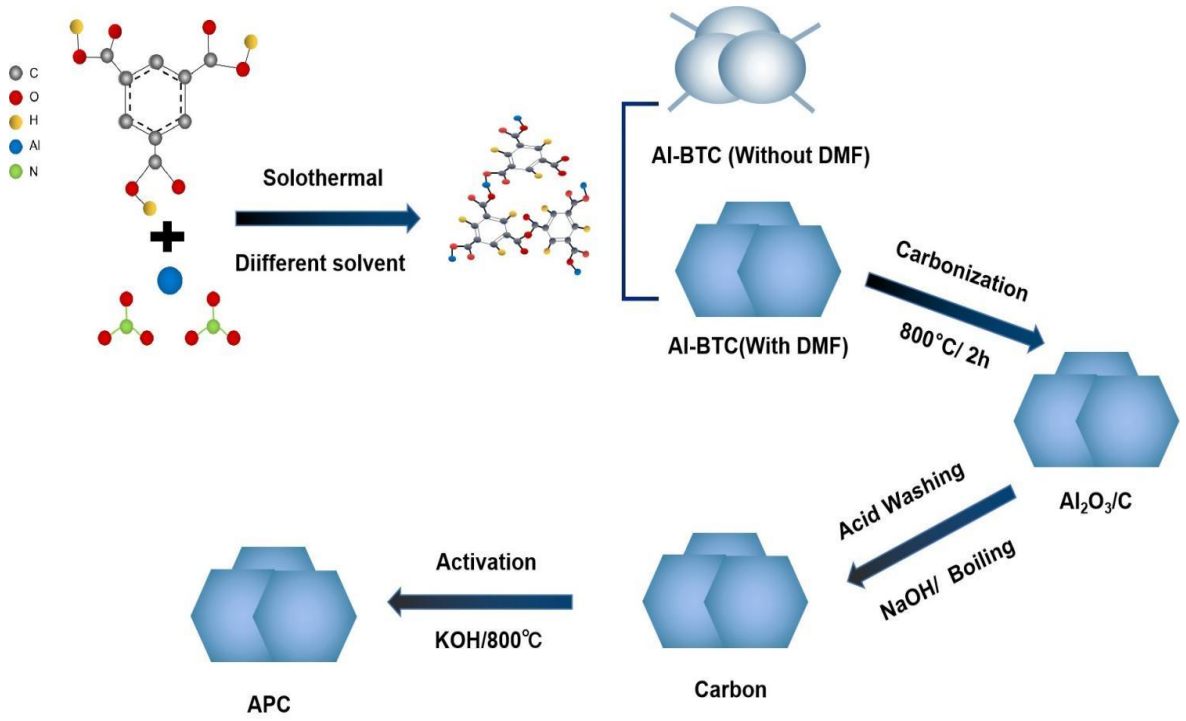

Figure 1. Schematic illustration of the preparation of APC-800

Finally, the chemical activation was executed by mixing the prepared sample and KOH with 1:3 mass ratios. It was directly activated in a nitrogen-filled tube furnace at 800 °C for 1 h. The resultant product denoted as APC-800 was washed with deionized water and dried for later use. The schematic illustration of the preparation of APC-800 is displayed in Fig. 1.

2.2. Characterization techniques

The surface morphology and crystalline structure of the obtained carbon samples are characterized by characterization techniques such as SEM, HR-TEM, XRD, Raman, BET and XPS.

2.3. Electrochemical analysis

For the making of the working electrode: 100mg APC-800 and 25mg expanded graphite was ground fully for 20 min, then added 25mg of PTFE (feeding ratio is 4: 1: 1), continue to grind until pressed into a thin sheet. The sheet was further pressed by a roller press until the thickness of the sheet was 50μm. A piece of 1×1 cm^2 size was cut and pressed on nickel foam with a tablet press machine, and welded with nickel wire to get a carbon working electrode.

The electrochemical test was performed under a 3-electrode system which contains a reference electrode of Zn/ZnO electrode, carbon working electrode, and a 1×1 cm^2 nickel ring as the counter electrode, 6M KOH solution as electrolyte. Galvanostatic charge-discharge (GCD) and cyclic voltammetry (CV) were investigated in the potential range of 0.4 - 1.4 V (vs. Zn/ZnO) by a LAND

3001A battery test system and CHI760D electrochemical workstation, respectively. The specific capacitances are calculated from the GCD curves according to the following equation:

$$C=It/mV \quad (1)$$

Here, C, t, I and V represent the specific capacitance (F g^{-1}), discharge time(s), discharge current (A) and voltage interval (V) of the APC, respectively.

3. RESULT AND DISCUSSION

3.1. Material morphology and structural characterization

As shown in Fig. 2, the contained elements of Al-BTC, Al_2O_3/C, Al-BTC-C and APC-800 were analyzed by element mapping analysis. As seen from Fig.2a, Al-BTC includes a mass of O, C and Al elements. The elements of Al and O are significantly reduced by the KOH treatment and activation of APC, and the elemental distribution of C is basically unchanged. (Fig.2d).

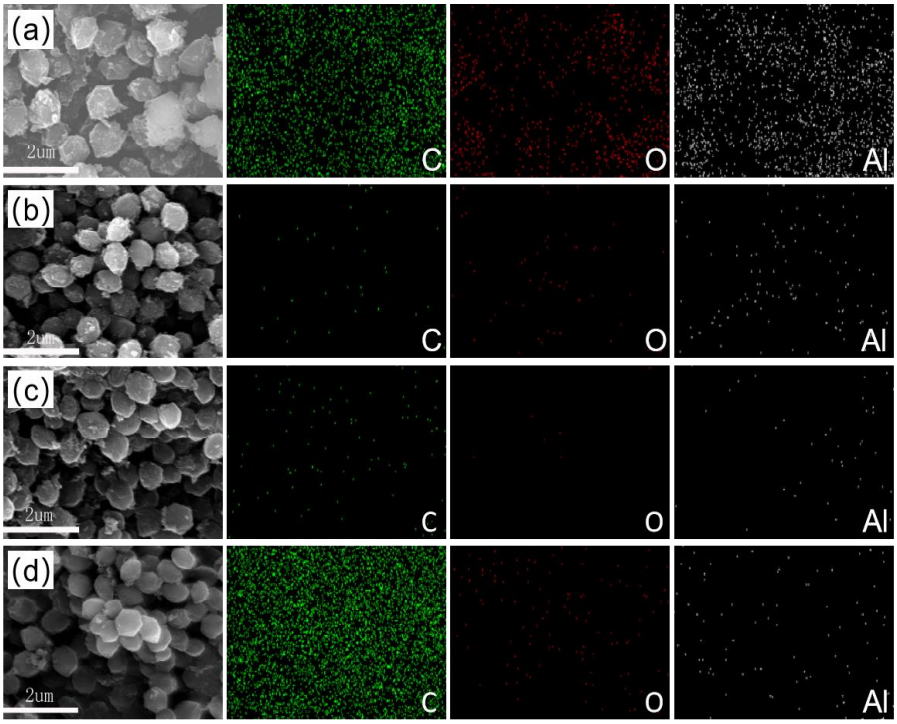

Figure 2. Element mapping images of (a) Al-BTC; (b) The composite of Al_2O_3/C obtained by carbonating Al-BTC; (c) Carbon obtained by boiling Al_2O_3/C with 8 M NaOH solution: (d) APC-800 obtained by mixing calcination of carbon and KOH at 800 ℃.

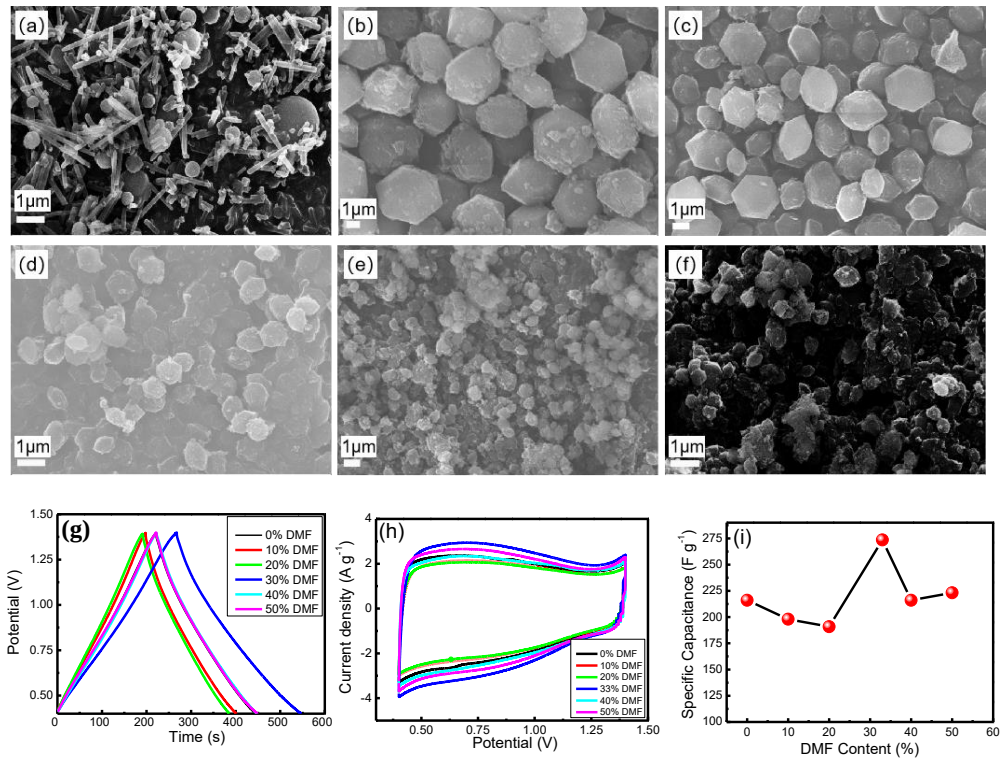

Figure 3. SEM images of Al-BTC (a) 0% DMF; (b) 10% DMF; (c) 20% DMF; (d) 33% DMF; (e) 40% DMF; (f) 50% DMF; (g) GCD curves of Al-BTC with different DMF content at 1A g^{-1}; (h) CV curves of APC with different DMF contents at 10mV s^{-1} ; (i) Line chart of specific capacitance of APC with different DMF content at 1A g^{-1}.

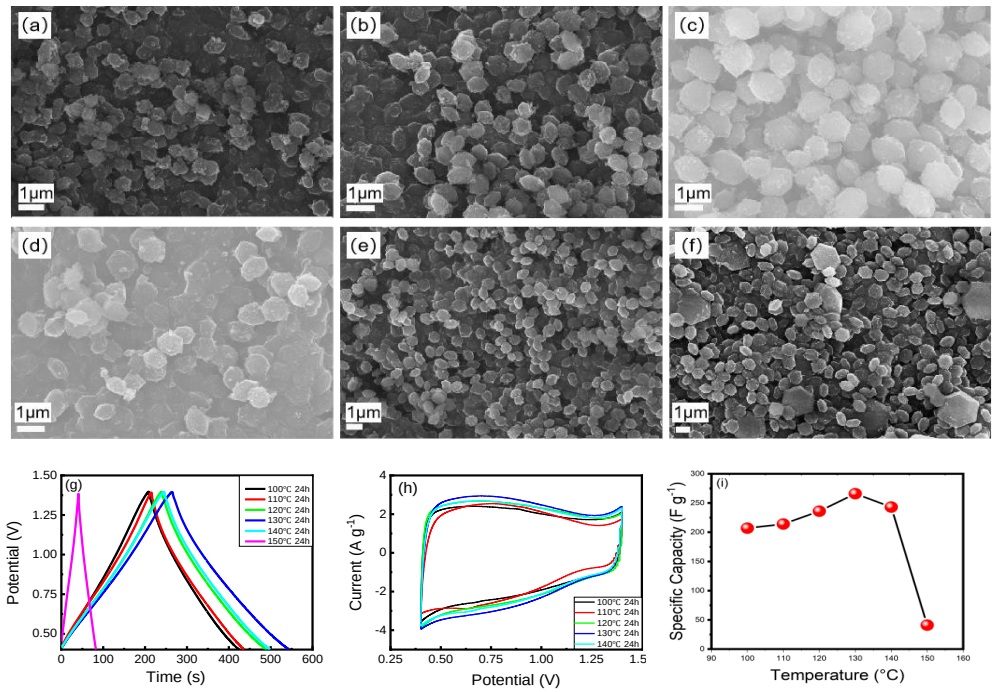

Figure 4. SEM images of Al-BTC (a) 100℃; (b) 110℃; (c) 120℃;(d) 130℃; (e) 140℃; (f) 150℃; (g) GCD curves of Carbon with different reaction temperature at 1A g^{-1}; (h) CV curves of Carbon reaction temperature at 10 mV s^{-1} ; (i) Line chart of specific capacity of Carbon with reaction temperature at 1A g^{-1}.

Fig. 2(a) demonstrates that the as-prepared Al-BTC has a hexagon morphology. Moreover, the key factors of the addtion of DMF, reaction temperature and time on the morphology of Al-BTC are shown in Fig. 3 and Fig. 4, respectively. As given in Fig. 2(b), the sample keeps its hexagonal shape and smooth surface after boiling in the 6 M KOH solution as compared to the previous treatment. The mesopores are enriched by increasing the SSA of carbon by removing Al_2O_3 particles, thereby facilitating the penetration of electrolyte ions in the reaction and further improving the electrochemical properties of the material. In order to enhance the electrochemical performance of carbon materials, KOH is used as an activator to activate carbon materials due to its environmental protection and resource abundance. Compared to the untreated precursors, the APC surface becomes smoother after KOH activation at 800℃ as shown in Fig. 2(d).

We have explored the impacts of different solvent ratios, reaction temperature and time on the electrochemical performance of Al-BTC to obtain APC with the best electrochemical properties. Among these factors, the content of DMF in the solvent has the greatest influence on the morphology of the prepared Al-BTC. It is shown that the addition of DMF in the solvent has a huge effect on the morphology of Al-BTC (Fig. 3). The shape of Al-BTC is spherical, and some sticks are attached to the side without the addition of DMF. After the addition of DMF, Then the shapes of Al-BTC changed from spherical to hexagonal with the addition of DMF, revealing its surface has a huge influence on the nucleation growth process of Al-BTC. When the DMF content in the solvent is 10%, the side length of the hexagon is about 2,100 nm; when the DMF content is 20%, the side length of the hexagon is about 1,600 nm; when the DMF content is 33%, the hexagon The side length is about 440 nm.

Additionally, the reaction temperature has a certain effect on the morphology of Al-BTC. When the temperature rises above 110°C, the morphology of Al-BTC will change from irregular blocks to hexagons. Meanwhile, the effect of the reaction time is not obvious on the prepared Al-BTC.

3.2. Electrochemical performance

As seen from Fig. 3 (b-d), as the DMF content increases, the volume of Al-BTC gradually decreases. It can be seen from Fig. 3 (e-f) that when the DMF content continued to increase, the nucleation and growth process of Al-BTC began to appear disordered, and the hexagon gradually disappeared, forming large irregular lumps. The appropriate amount of DMF can induce Al-BTC to grow in different directions. However, the extra high content of DMF will inhibit its growth. As shown in Fig. 3 (g-i), the results demonstrate that the volume ratio of DMF to the total solvent is 33% (ie ethanol: deionized water: DMF is 1: 1: 1) is the optimal ratio for the preparation of hexagonal APC with the highest specific capacitance of 273 F g^{-1}. The SEM images also reveal that the smallest hexagonal Al-BTC is obtained when the content of DMF is 33%. The smaller volume is beneficial to increase the contact area with the electrolyte. It is also easier to form an expanded electric double layer interface with higher specific capacitance.

Similarly, the SEM images and GCD profiles of the obtained Al-BTC at different reaction temperatures are shown in Fig. 4. The obtained samples show basically the same hexagonal shape with their side length between 400-450 nm when the reaction temperature is 100-150 ℃. As shown in Fig.4, when the reaction temperature is 100 ℃, only an irregular shape is formed, which indicates that the reaction temperature should be higher than 110℃ to form a hexagonal shape. Subsequently, the GCD tests reveal the synthesized APC at 130 ° C has the highest SC (280 F g^{-1}).

The above results indicate the ratio of the solvent is a prominent factor in these conditions. So, the optimal conditions for the hexagonal Al-BTC with higherst electrochemical performance are as follows: DMF content in the solvent is 33% (i.e. water: ethanol: DMF is 1: 1: 1), the reaction temperature is 130 degrees, and the reaction time is 12h.

The CV test was carried out at a scan rate of 1-1,000 mV s^{-1}, and the collected curves exhibit quasi-rectangular shapes, and a slight deformation occurs at 1,000 mV s^{-1}, which indicates that the maximum tolerable scan rate of APC-800 is 500 mV s^{-1} (Fig. 5). As calculated from the CV curve at 1mV s^{-1}, we can obtain that the SC of APC can reach 320 F g^{-1}. As the scan rate increases, the SC decreases with the increasing scan speed. The material can withstand a scan rate of 500 mV s^{-1}, showing excellent rapid responseability. The GCD curves in Fig. 5c show well-paired triangles, indicating the excellent capacitance behavior of carbon materials. Fig. 5d shows GCD curves at the high current densities of 20-100 A g^{-1}, which is complementary to Fig. 5c. The sample provides a specific capacitance of 324 F g^{-1} at 1 A g^{-1}, much higher than the reported materials in some respected journals [32-35].

The cycle performance of the obtained carbon material has been studied by CV tests at 200 mV s^{-1} for 10,000 cycles and GCD tests at 50 A g^{-1} for 1.5×10^5 cycles. As seen in Fig. 5e, all quasi-rectangular curves almost completely coincide, meaning superior durability. In particular, the curve still maintains a similar quasi-square shape after 10,000 cycles and almost overlaps with the first cycle, demonstrating superior durability. Fig. 5f indicates that the SC of APC remained stable, and only a slight loss (4%) occurs after the long-term GCD test of 1.5×10^5 cycles, showing its excellent cycling ability. Furthermore, APC can offer superior cycling ability and specific capacitance than the reported carbon materials as compared with some previous reported carbon materials derived from MOF in the literatures, as shown in Table 1.

Table 1. The comparison of the supercapacitors performance in APC and other porous carbons described in the literature

Supercapacitor Electrode	Specific Capacitance	Current Density	Cycling Stability (%)	Cycles
UCN-20-750 [32]	256 F g^{-1}	1 A g^{-1}	91%	10,000
All-solid-state symmetric super-capacitor [33]	150.8 F g^{-1}	5 A g^{-1}	94.8%	10,000
MOF-5 [34]	300 F g^{-1}	1.5 A g^{-1}	91.5%	3,000
HPNCs/rGO-00[35]	245 F g^{-1}	1 A g^{-1}	90%	10,000
This work	324 F g^{-1}	1 A g^{-1}	96%	150,000

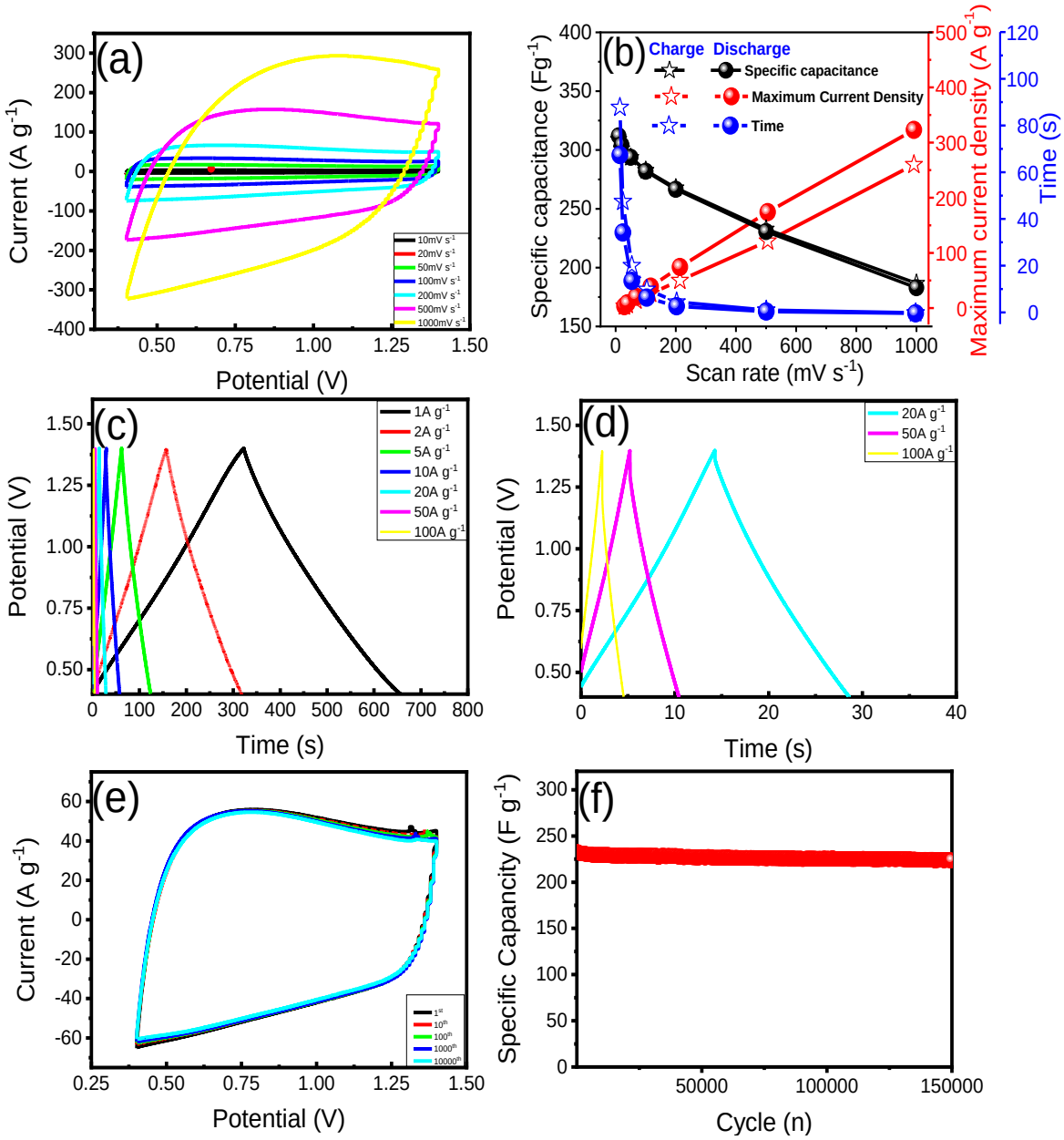

Figure 5. (a) CV curves of APC at different scan rates from 1 to 1,000 mV s^{-1}; (b) the obtained electrochemical parameters of APC electrode from CV tests; (c, d) GCD curves of APCat different current densities (1-100 A g^{-1}); (e) CV curves of APC electrode at 200 mV s^{-1} for 10,000 cycles; (f) Specific capacitance retention of APC electrode for 1.5×10^5 cycles at 100 A g^{-1}.

4. CONCLUSION

In this work, hexagonal coin-shaped Al-MOF and APC were prepared by controlling the ratio of ethanol, water and DMF solvent. This study has shown that DMF has an important effect on the morphology of Al-MOF, in which the addition of 20-33% in the solvent can promote the transformation of Al-MOF from spherical to hexagonal, and the excessive amount of DMF will cause Al-MOF to shape failure. In addition, electrochemical tests show that the samples with DMF content

of 30% and reaction temperature of 130 °C for 12 h have the best electrochemical performance. The sample provides a specific capacitance of 324 F g^{-1} at 1 A g^{-1}, and it still retains 96% of the initial capacity after 150,000 cycles, showing superior electrochemical performance. This study offers a significant research basis for the future design, regulation, and optimization of the morphology and electrochemical properties of MOF-derived carbon materials.

References

1. X. Liu, S. Li, R. Mi, J. Mei, L.-M. Liu, L. Cao, W.-M. Lau, H. Liu, *Applied Energy*, 153 (2015) 32–40.
2. S. Rehman, L.M. Al-Hadhrami, M.M. Alam, *Renewable & Sustainable Energy Reviews*, 44 (2015) 586–598.
3. E. Fumagalli, *Nature Energy*, 1 (2016) 16096.
4. S. Koohi-Fayegh, M.A. Rosen, *Journal Of Energy Storage*, 27 (2020), 101047.
5. B. Li, P. Gu, Y. Feng, G. Zhang, K. Huang, H. Xue, H. Pang, *Advanced Functional Materials*, 27 (2017) 1605784.
6. F. Yi, H. Ren, K. Dai, X. Wang, Y. Han, K. Wang, K. Li, B. Guan, J. Wang, M. Tang, J. Shan, H. Yang, M. Zheng, Z. You, D. Wei, Z. Liu, *Energy & Environmental Science*, 11 (2018) 2016–2024.
7. J. Park, W. Kim, *Advanced Energy Materials*, 11 (2021), 2170107.
8. D. Qi, Y. Liu, Z. Liu, L. Zhang, X. Chen, *Advanced Materials*, 29 (2017) 1602802.
9. Q. Wu, T. He, Y. Zhang, J. Zhang, Z. Wang, Y. Liu, L. Zhao, Y. Wu, F. Ran, *Journal Of Materials Chemistry* A, 9 (2021) 24094–24147.
10. S.J. Yoo, B. Evanko, X. Wang, M. Romelczyk, A. Taylor, X. Ji, S.W. Boettcher, G.D. Stucky, *Journal Of The American Chemical Society*, 139 (2017) 9985– 9993.
11. E. Frackowiak, Q. Abbas, F. Béguin, *Journal Of Energy Chemisty*, 22 (2013) 226–240.
12. Y. Lei, W. Qin, Z. Peixin, Z. Junmin, W. Dongrui, L. Yongliang, R. Xiangzhong, M. Hongwei, D. Libo, Z. Zijian, *Advanced Materials*, 30 (2018) 1706054.
13. B.K. Saikia, S.M. Benoy, M. Bora, J. Tamuly, M. Pandey, D. Bhattacharya, *Fuel*, 282 (2020), 118796.
14. J. Wang, J. Tang, B. Ding, V. Malgras, Z. Chang, X. Hao, Y. Wang, H. Dou, X. Zhang, Y. Yamauchi, *Nature Communications*, 8 (2017) 15717.
15. Y. Zhang, L. Cheng, L. Zhang, D. Yang, C. Du, L. Wan, J. Chen, M. Xie, *Journal Of Energy Storage*, 34 (2021), 102018.
16. L. Haowen, F. Dongying, Z. Xian-Ming, *Royal Society Open Science*, 5 (2018) 171028–171039.
17. L. Xueqin, H. Changlong, T. Bochong, W. Yue, L. Mei, W. Yuanwei, Z. Yihua, L. Chenguang, T. Zhiyong, *Nanoscale*, 9 (2017) 2187–2196.
18. W. Kang, Y. Zhang, L. Fan, L. Zhang, F. Dai, R. Wang, D. Sun, *ACS Applied Materials& Interfaces,* 9 (2017) 10602–10609.
19. X.-C. Xie, K.-J. Huang, X. Wu, *Journal Of Materials Chemistry* A, 6 (2018) 6754–6771.
20. Y. Wang, L. Tao, Z. Xiao, R. Chen, Z. Jiang, S. Wang, *Advanced Functional Materials*, 28 (2018) 1705356.
21. S. Zhao, Y. Long, X. Shen, S. Wang, Y. Su, X. Zhang, Z. Zhang, *Science Of The Total Environment,* 799 (2021), 149497.
22. P. Horcajada, T. Chalati, C. Serre, B. Gillet, C. Sebrie, T. Baati, J.F. Eubank, D. Heurtaux, P. Clayette, C. Kreuz, J.S. Chang, Y.K. Hwang, V. Marsaud, P.N. Bories, L. Cynober, S. Gil, G. Ferey, P. Couvreur, R. Gref, *Nature Materials*, 9 (2010) 172–178.
23. R.J. Kuppler, D.J. Timmons, Q.-R. Fang, J.-R. Li, T.A. Makal, M.D. Young, D. Yuan, D. Zhao, W. Zhuang, H.-C. Zhou, *Coordination Chemistry Reviews*, 253 (2009) 3042–3066.
24. Y. Cuiping, W. Yan, C. Jiewu, Y. Dongbo, Z. Xinyi, S. Xia, Z. Jianfang, Z. Yong, V. Robert, M.A.

Pulickel, W. Yucheng, *Journal Of Materials Chemistry* A, 6 (2018) 8396–8404.
25. L.E. Kreno, K. Leong, O.K. Farha, M. Allendorf, R.P. Van Duyne, J.T. Hupp, *Chemical Review*, 112 (2012) 1105–1125.
26. A. Indra, T. Song, U. Paik, *Advanced Materials*, 30 (2018) 1705146.
27. C. Wang, T. Liu, *RSC Advances*, 6 (2016) 105540–105549.
28. S. Yongming, W. Li, L. Yanbin, L. Yuzhang, H.R. Lee, P. Allen, H. Xiangming, C. Yi, J*oule*, 3 (2019) 1080–1093.
29. J.-K. Sun, Q. Xu, *Energy & Environmental Science*, 7 (2014) 2071–2100.
30. J. Sun, A. Klechikov, C. Moise, M. Prodana, M. Enachescu, A.V. Talyzin, *Angewandte Chemie*, 57 (2018) 1034–1038.
31. S. Li, Q. Zhang, C. Yin, J. Chen, X. Yang, S. Wang, *Journal Of Cleaner Production*, 292 (2021), 125998.
32. M. Liu, F. Zhao, D. Zhu, H. Duan, Y. Lv, L. Li, L. Gan, *Materials Chemistry And Physics*, 211 (2018) 234–241.
33. F. Yu, T. Wang, Z. Wen, H. Wang, *Journal Of Power Sources*, 364 (2017) 9–15.
34. I.A. Khan, A. Badshah, I. Khan, D. Zhao, M.A. Nadeem, *Microporous And Mesoporous Materials*, 253 (2017) 169–176.
35. L. Xin, Q. Liu, J. Liu, R. Chen, R. Li, Z. Li, J. Wang, *Electrochimica Acta*, 248 (2017) 215–224.